A variational analysis for the moving finite element method for gradient flows

Xianmin Xu*

July 14, 2021

Abstract

By using the Onsager principle as an approximation tool, we give a novel derivation for the moving finite element method for gradient flow equations. We show that the discretized problem has the same energy dissipation structure as the continuous one. This enables us to do numerical analysis for the stationary solution of a nonlinear reaction diffusion equation using the approximation theory of free-knot piecewise polynomials. We show that under certain conditions the solution obtained by the moving finite element method converges to a local minimizer of the total energy when time goes to infinity. The global minimizer, once it is detected by the discrete scheme, approximates the continuous stationary solution in optimal order. Numerical examples for a linear diffusion equation and a nonlinear Allen-Cahn equation are given to verify the analytical results.

1 Introduction

The moving finite element method(MFEM) was first developed in [28, 27] about forty years ago. It is a typical r-type adaptive method[17, 7, 22, 34, 6], where the mesh vertexes are relocated without changing the mesh topology. In the MFEM, the mesh relocation is done by solving a dynamic equation for the vertexes coupled with the original partial differential equations. No interpolation is needed in the method since the mesh is continuous with time. The MFEM has arisen considerable interest and has been further developed in several directions(c.f [1, 16, 8, 36, 2, 3] among many others).

However, like all other r-adaptive methods, the theoretical analysis for the MFEM is far from being complete. The first error analysis for MFEM was done by Dupont [16], where he proved the optimal convergence of the method for a linear convection diffusion equation when the solution is smooth. This is not enough since we are more interested in non-smooth solutions for adaptive methods. Later on, Jimack proved the locally optimal approximation for the stationary solution of a linear parabolic equation without the smoothness assumption[19, 20, 21]. In this study, we aim to do analysis for a nonlinear gradient flow system by using the Onsager variational principle as an approximation tool. Recently, a similar energetic variational approach is used to develop interesting Lagrangian schemes for some gradient flow systems [9, 24, 23].

*LSEC, Institute of Computational Mathematics and Scientific/Engineering Computing, NCMIS, AMSS, Chinese Academy of Sciences, Beijing 100190, China; School of Mathematical Sciences, University of Chinese Academy of Sciences, Beijing 100049, China (xmxu@lsec.cc.ac.cn).

The Onsager variational principle is a fundamental principle for irreversible thermodynamic processes in statistical physics[29, 30, 14]. It has be used to model many dissipative physical systems[13, 14], such as the Stokes equation in hydrodynamics, the Ericksen-Leslie equation in liquid crystal, and the GNBC boundary condition for moving contact lines[33], etc. Recently, the Onsager principle has been used as an approximation tool for many problems in two-phase flows and in material science[15, 37, 12, 26, 38, 18]. In particular, it has been used to derive an efficient numerical method for wetting dynamics[25].

In this work, we first give a new derivation of the MFEM for a gradient flow system by using the Onsager principle as an approximation tool. The key idea is to approximate the system in a nonlinear approximation space of free-knot piecewise polynomials[10]. Both the mesh vertexes and the nodal values of the finite element function are regarded as unknowns. We derive a system of ordinary differential equations(ODEs) for them. The ODE system coincides with the discrete equation of the MFEM, which has been derived in a totally different way in [28]. Here we do not need to compute the multiply of a Dirac measure and a discontinuous function, so that the "mollification" technique or any other formally calculation is not needed. Furthermore, our derivation shows that the discretized problem has the same energy dissipation structure of the continuous system. This makes us to prove the energy decay property of the discrete problem easily.

Based on the variational formula, we do error analyse for the MFEM for a stationary solution of the gradient flow system. The analysis can be regarded as a generalization of the results in [20] to nonlinear equations. We show that the MFEM gives locally best approximations to the energy. When a global minimizer is detected, an optimal error estimate is proved using the nonlinear approximation theory. Numerical examples show that the optimal convergence can be obtained for a linear diffusion equation and for stationary solutions of a nonlinear Allan-Cahn equation. In this paper, we mainly consider the one dimensional problem. All the results can be generalized to higher dimensional cases directly.

The structure of the paper is as follows. In section 2, we introduce the Onsager variational principle and show that it can be used to derive the partial differential equation model for a gradient flow system. In Section 3, we derive the MFEM by using the Onsager principle as an approximation tool. In Section 4, we do error analysis for the stationary solution of a nonlinear reaction diffusion equation. Some numerical examples are illustrated to verify the analytical results in the last section.

2 The Onsager variational principle for a gradient flow system

2.1 The Onsager principle

Suppose a physical system is described by a time dependent function u. For simplicity, we denote by $\dot{u} = \frac{\partial u}{\partial t}$ the time derivative of u. For a dissipated system, the evolution of u can dissipate energy. The dissipation function is defined as half of the total energy dissipated with respect to the flux $\dot{u}$(c.f. [14]). For a simple gradient flow system, we assume the dissipation function is

$$\Phi(\dot{u}) = \frac{\xi}{2}\|\dot{u}\|^2, \tag{1}$$

where ξ is a positive friction coefficient determined by the dissipation processes of a physical system and $\|\cdot\|$ is a L^2 norm.

Suppose that the free energy of the system is given by a functional $\mathcal{E}(u)$. For given $\dot{u}$, the rate of change of the total energy is calculated by

$$\dot{\mathcal{E}}(u;\dot{u}) = \langle \frac{\delta \mathcal{E}(u)}{\delta u}, \dot{u} \rangle. \tag{2}$$

Then a Rayleighian (functional) is defined as

$$\mathcal{R}(u;\dot{u}) = \Phi(\dot{u}) + \dot{\mathcal{E}}(u;\dot{u}). \tag{3}$$

With these definitions, the Onsager principle can be stated as follows([14]). For any given u at the present time, the time derivative $\dot{u}$ is obtained by minimizing the Rayleighian among its all possible choices. In other words, the evolution equation of u is determined by minimizing the Rayleighian $\mathcal{R}(u,\dot{u})$ with respect to $\dot{u}$, i.e.

$$\min_{\dot{u}\in V} \mathcal{R}(u,\dot{u}). \tag{4}$$

Here V is the admissible space of $\dot{u}$. Since the Rayleighian is a quadratic form with respect to $\dot{u}$, the problem (4) is equivalent to its Euler-Lagrange equation

$$\xi(\dot{u},\psi) = -\langle \frac{\delta \mathcal{E}(u)}{\delta u}, \psi \rangle, \qquad\qquad \forall \psi \in V, \tag{5}$$

or in a simple form,

$$\xi \dot{u} = -\frac{\delta \mathcal{E}(u)}{\delta u}. \tag{6}$$

In physics, the equation indicates a balance between the friction force $-\xi\dot{u}$ and the general driven force $\frac{\delta \mathcal{E}(u)}{\delta u}$. The equation (6) can be simply rewritten as a gradient flow equation,

$$\frac{\partial u}{\partial t} = -\xi^{-1}\frac{\delta \mathcal{E}(u)}{\delta u}. \tag{7}$$

It is easy to see that the solution u of Equation (5)(or (7)) satisfies the following energy decay property

$$\frac{d\mathcal{E}(u)}{dt} \le 0. \tag{8}$$

Actually, by setting $\psi = \frac{\partial u}{\partial t}$ in (5), we have

$$\frac{d\mathcal{E}}{dt} = \langle \frac{\delta \mathcal{E}(u)}{\delta u}, \frac{\partial u}{\partial t} \rangle = -\xi \| \frac{\partial u}{\partial t} \|_V^2 = -2\Phi(\dot{u}) \le 0. \tag{9}$$

The rate of decreasing of the total energy is equal to twice of the dissipation function.

2.2 The model problem

For simplicity in presentations, we mainly consider a specific gradient flow system in this paper, which corresponds to a (nonlinear) reaction diffusion equation.

Denote by Ω a domain in R^n. Suppose the energy functional is given by

$$\mathcal{E}(u,\nabla u) = \int_\Omega \frac{\alpha}{2}(\nabla u)^2 + F(x,u)dx, \tag{10}$$

where $\alpha > 0$ is the diffusion coefficient and $F(x,u)$ is a function with respect to x and u. We assume that $u \in H_0^1(\Omega)$ and $\dot{u} \in L^2(\Omega)$. The dissipation function is given by

$$\Phi(\dot{u}) = \frac{\xi}{2}\int_\Omega \dot{u}^2 dx, \tag{11}$$

with a positive friction coefficient ξ. Then the Rayleighian is calculated as

$$\mathcal{R}(u,\dot{u}) = \Phi(\dot{u}) + \dot{\mathcal{E}} = \frac{\xi}{2}\int_\Omega \dot{u}^2 dx + \int_\Omega \alpha\nabla u\cdot\nabla\dot{u} + \partial_u F(x,u)\dot{u}dx. \tag{12}$$

We minimize $\mathcal{R}$ with respect to $\dot{u}$.

By integral by part, $\mathcal{R}$ is rewritten as

$$\mathcal{R}(u,\dot{u}) = \frac{\xi}{2}\int_\Omega \dot{u}^2 dx + \int_\Omega [-\alpha\Delta u + \partial_u F(x,u)]\dot{u}dx.$$

The corresponding Euler-Langrange equation of (12) is

$$\partial_t u - \frac{\alpha}{\xi}\Delta u + \frac{1}{\xi}f(x,u) = 0, \tag{13}$$

where $f(x,u) = \partial_u F(x,u)$. It is a quasi-linear reaction diffusion equation. Some typical examples include the linear diffusion equation(when $F = 0$) and the Allen-Cahn equation(when F is a double-well function), etc.

In general, we assume that $f(x,u)$ is Liptchitz continuous with respect to u, i.e.

$$|f(x,v) - f(x,w)| \le L_0|v-w|, \qquad \forall v, w, \tag{14}$$

for some constant $L_0 > 0$. Under this condition and some assumption on the domain Ω, the equation (13) has a unique solution (c.f. Theorem 5.1 in [31]).

3 Derivation of the moving finite element method by the Onsager Principle

The Onsager principle can be used to derive numerical methods for the model problem (13). The idea is as follows. We choose a finite dimensional subspace V_h of $H_0^1(\Omega)$. For a time dependent function $u_h(t,x) \in V_h$, we can compute the energy functional $\mathcal{E}(u_h)$ and the dissipation function $\Phi(\dot{u}_h)$. By minimizing the discrete Rayleighian $\mathcal{R}(u_h;\dot{u}_h) := \dot{E}(u_h;\dot{u}_h) + \Phi(\dot{u}_h)$ with respect to $\dot{u}_h$, we obtain a dynamic equation for $u_h(t,x)$, which is a (semi-)discrete problem for (13). For example, if we choose V_h as a standard Lagrangian finite element space, it is easy to verify that we can obtain a finite element problem same as that derived by the standard Galerkin approach. In the following, we choose V_h as a nonlinear approximation space composed of free-knot piecewise polynomials. Then we derive the MFEM proposed in [28].

For simplicity in notations, we consider only the one-dimensional problem hereinafter. The domain Ω is simply a bounded interval $I = (a,b)$. The model problem (13) is reduced to

$$\partial_t u - \frac{\alpha}{\xi}\partial_{xx} u + \frac{1}{\xi}f(x,u) = 0. \tag{15}$$

3.1 Nonlinear approximation space

We recall some known results on the nonlinear approximation space of the piecewise linear functions with free-knots [10]. Let N be a positive integer and let

$$X := \{a =: x_0 < x_1 < \cdots < x_N := b\}$$

be a set of ordered points in the interval $\bar{I} = [a, b]$. This generates a partition of I, which we denote as $\mathcal{T}(X) := \{I_k\}_{k=1}^N$, where $I_k = (x_{k-1}, x_k)$. Let

$$V_h(X) := \{v_h \in C([a,b]) | v_h \text{ is linear in } I_k, \forall k = 1, \cdots, N\}, \tag{16}$$

be the standard piecewise linear finite element space with respect to the partition $\mathcal{T}(X)$. Denote by V_h^N the space with N intervals as follows

$$V_h^N := \cup_{\#(X)=N+1} V_h(X), \tag{17}$$

where $\#(X)$ denotes the cardinality of X. It is a function space for piecewise linear functions with free knots $\{x_k\}$. Notice that V_h^N is not a linear space, since the summation of two functions in V_h^N may not belongs to the same space when they correspond to different partitions X.

For any function $u_h(x) \in V_h^N$, it can be written as

$$u_h(x) = \sum_{k=1}^{N-1} u_k \phi_k(x), \tag{18}$$

where $\phi_k(x)$ is the standard nodal basis function with respect to a partition $\mathcal{T}(X)$, namely

$$\phi_k(x) = \frac{x - x_{k-1}}{x_k - x_{k-1}} \chi_{I_k}(x) + \frac{x_{k+1} - x}{x_{k+1} - x_k} \chi_{I_{k+1}}(x),$$

where χ_{I_k} is the characteristic function corresponding to I_k,

$$\chi_{I_k}(x) = \begin{cases} 1 & \text{if } x \in I_k \\ 0 & \text{otherwise.} \end{cases}$$

In Equation (18), both u_k and x_k ($k = 1, \cdots, N-1$) can change their values. Therefore, V_h^N is a $2(N-1)$ manifold. We remark that V_h^N is not a smooth manifold in general. There exists some function $u_h \in V_h^N$ which corresponds to many different coordinates $\{u_k, x_k \mid k = 1, \cdots N-1\}$. In this sense, the manifold degenerates for some functions in V_h^N.

The nonlinear approximation theory for free-knot piecewise linear polynomials has been studied extensively (c.f. [32, 10] and the reference therein). For a function $u \in H_0^1$, the best approximation of u in V_h^N in energy norm is defined as

$$\sigma_N(u) = \inf_{v_h \in V_h^N} |u - v_h|_{H^1}. \tag{19}$$

Here $|u|_{H^1} := \left(\int_I (\partial_x u)^2 dx \right)^{\frac{1}{2}}$ is the standard H^1 semi-norm.

To characterize the approximation property of functions in V_h^N, it is convenient to use the Besov spaces. We denote by $B_q^r(L_q(I))$ a standard Besov space. We will not give the details of the definitions of the Besov space here, but refer to [35, 11]. We only mention that $B_q^r(L_q(I))$ is a space consisting of functions with smoothness order r measured in L_q. When $q = 2$, $B_2^r(L_2(I))$ is identical to the Sobolev space H^r. The following lemma is known from the literature(c.f. [5, 4]).

Lemma 3.1. *If $u \in B_q^{s+1}(L_q(I))$ with $0 \le s \le 1$ and $1/q < s + 1/2$, then we have*

$$\sigma_N(u) \le CN^{-s}|u|_{B_q^{s+1}(L_q(I))}. \tag{20}$$

The lemma is a one-dimensional version of Theorem 9.1 in [4]. The proof of the lemma can be found in [5]. By this lemma, the best approximation in energy norm of a (one-dimensional) function by a free-knot piecewise linear function is of order $O(N^{-1})$.

3.2 The moving finite element method

Consider a time dependent function $u_h(t,x) = \sum_{k=1}^{N-1} u_k(t)\phi_k(t,x)$ in V_h^N, where

$$\phi_k(t,x) = \frac{x - x_{k-1}(t)}{x_k(t) - x_{k-1}(t)}\chi_{I_k}(x) + \frac{x_{k+1}(t) - x}{x_{k+1}(t) - x_k(t)}\chi_{I_{k+1}}(x), \tag{21}$$

is the nodal basis function corresponding to a time dependent partition $\mathcal{T}(X(t))$ and the set $X(t)$ is given by

$$X(t) := \{a = x_0 < x_1(t) < \cdots < x_{N-1}(t) < x_N = b\}.$$

In the partition, the interior notes $x_k(t), k = 1, \cdots, N-1$, may change positions when time t evolves. In the formula of $u_h(t,x)$, there are $2(N-1)$ time dependent parameters

$$\{u_k(t), x_k(t) \mid k = 1, \cdots N-1\}. \tag{22}$$

We aim to approximate the solution u of the model problem (15) by a discrete function $u_h(t,x)$. For that purpose, we will derive a dynamic equation for $u_k(t)$ and $x_k(t)$ by using the Onsager principle. The derivation is similar to that for continuous problems in Section 2.

We first compute the discrete energy functional and the discrete dissipation function as follows. Notice that the time derivative and space derivative of $u_h(t,x)$ are given by

$$\begin{aligned}
\partial_t u_h &= \sum_{k=1}^{N-1} (\dot{u}_k(t)\phi_k(t,x) + \dot{x}_k(t)\beta_k(t,x)),\\
\partial_x u_h &= \sum_{k=1}^{N-1} u_k(t)\partial_x\phi_k(t,x),
\end{aligned}$$

where

$$\beta_k(t,x) = \frac{\partial u_h}{\partial x_k} = -D_h u_{k-1}\frac{x - x_{k-1}(t)}{x_k(t) - x_{k-1}(t)}\chi_{I_k}(x) - D_h u_k \frac{x_{k+1}(t) - x}{x_{k+1}(t) - x_k(t)}\chi_{I_{k+1}}(x),$$

with $D_h u_k = \frac{u_{k+1}(t) - u_k(t)}{x_{k+1}(t) - x_k(t)}$. Then the discrete energy functional $\mathcal{E}$ with respect to u_h is calculated by

$$\mathcal{E}_h(u_1, \cdots, u_{N-1}, x_1, \cdots, x_{N-1}) := \mathcal{E}(u_h) = \sum_{k=1}^{N} \int_{I_k} \frac{\alpha}{2}(\partial_x u_h)^2 + F(x, u_h)\mathrm{d}x. \tag{23}$$

It is a nonlinear function with respect to $\{u_k(t), x_k(t) \mid k = 1, \cdots N-1\}$. The discrete dissipation function is given by

$$\begin{aligned}
&\Phi_h(u_1, \cdots, u_{N-1}, x_1, \cdots, x_{N-1}; \dot{u}_1, \cdots, \dot{u}_{N-1}, \dot{x}_1, \cdots, \dot{x}_{N-1})\\
&:= \Phi(\partial_t u_h(t,x)) = \frac{\xi}{2}\int_I \Big(\sum_{k=1}^{N}(\dot{u}_k(t)\phi_k(t,x) + \dot{x}_k(t)\beta_k(t,x))\Big)^2 dx.
\end{aligned} \tag{24}$$

It is a quadratic function with respect to $\{\dot{u}_k(t), \dot{x}_k(t) \mid k = 1, \cdots N-1\}$.

We apply the Onsager principle for $\{\dot{u}_k(t), \dot{x}_k(t) \mid k = 1, \cdots N-1\}$. We minimize the discrete Rayleighian $\mathcal{R}_h$ with respect to $\dot{u}_k$ and $\dot{x}_k$:

$$\min_{\dot{u}_k, \dot{x}_k} \mathcal{R}_h := \Phi_h + \dot{\mathcal{E}}_h. \tag{25}$$

The problem is equivalent to its Euler-Lagrange equation

$$\begin{cases} \frac{\partial \Phi_h}{\partial \dot{u}_k} + \frac{\partial \mathcal{E}_h}{\partial u_k} = 0, & k = 1, \cdots, N-1; \\ \frac{\partial \Phi_h}{\partial \dot{x}_k} + \frac{\partial \mathcal{E}_h}{\partial x_k} = 0, & k = 1, \cdots, N-1. \end{cases} \tag{26}$$

This gives an ordinary differential system for $\{u_k(t), x_k(t) \mid k = 1, \cdots N-1\}$.

We now derive the explicit formula for the system (26). Denote $\mathbf{u} = (u_1, \cdots, u_{N-1})^T$ and $\mathbf{x} = (x_1, \cdots, x_{N-1})^T$. Notice that Φ_h is a quadratic function with respect to $\{\dot{u}_k(t), \dot{x}_k(t) \mid k = 1, \cdots N-1\}$. Then the equation (26) can be rewritten as

$$\begin{pmatrix} \mathbf{A} & \mathbf{B} \\ \mathbf{B} & \mathbf{C} \end{pmatrix} \begin{pmatrix} \dot{\mathbf{u}} \\ \dot{\mathbf{x}} \end{pmatrix} = \begin{pmatrix} \mathbf{f} \\ \mathbf{g} \end{pmatrix}. \tag{27}$$

The right hand side terms are given by

$$\mathbf{f} = (f_1, f_2, \cdots, f_{N-1})^T, \qquad \text{with}$$

$$f_k = -\frac{1}{\xi}\frac{\partial \mathcal{E}_h}{\partial u_k} = -\frac{1}{\xi}\int_I \alpha \partial_x u_h \partial_x \phi_k + f(x, u_h)\phi_k dx.$$

and

$$\mathbf{g} = (g_1, g_2, \cdots, g_{N-1})^T, \qquad \text{with}$$

$$g_k = -\frac{1}{\xi}\frac{\partial \mathcal{E}_h}{\partial x_k} = -\frac{1}{\xi}\Big(\int_I \alpha \partial_x u_h \partial_x \beta_k + f(x, u_h)\beta_k dx - \frac{\alpha}{2}[(\partial_x u_h)^2]|_{x_k}\Big),$$

where the jump $[(\partial_x u_h)^2]|_{x_k} := (\partial_x u_h)^2|_{I_k} - (\partial_x u_h)^2|_{I_{k-1}}$. The blocks $\mathbf{A}$, $\mathbf{B}$ and $\mathbf{C}$ in the coefficient matrix are $(N-1)\times(N-1)$ tridiagonal matrices, whose nonzero elements are functions of $\{u_k\}$ and $\{x_k\}$. Direct computations for the nonzero elements of $\mathbf{A}$ give

$$\begin{aligned} a_{k,k} &= \int_{I_k \cup I_{k+1}} \phi_k^2 dx, && k = 1, \cdots, N-1; \\ a_{k,k+1} = a_{k+1,k} &= \int_{I_{k+1}} \phi_k \phi_{k+1} dx, && k = 1, \cdots, N-2. \end{aligned}$$

This implies $\mathbf{A}$ is the mass matrix in the standard finite element method on a given triangulation $\mathcal{T}(X)$ with $X = \{a = x_0 < x_1 < \cdots < x_N = b\}$. The nonzero elements of the matrix $\mathbf{B}$ are computed as

$$\begin{aligned} b_{k,k} &= \int_{I_k \cup I_{k+1}} \phi_k \beta_k dx, && k = 1, \cdots, N-1; \\ b_{k,k+1} = b_{k+1,k} &= \int_{I_{k+1}} \phi_k \beta_{k+1} dx, && k = 1, \cdots, N-2. \end{aligned}$$

We can also compute the nonzero elements of the matrix $\mathbf{C}$,

$$c_{k,k} = \int_{I_k \cup I_{k+1}} \beta_k^2 dx, \qquad k = 1, \cdots, N-1;$$
$$c_{k,k+1} = c_{k+1,k} = \int_{I_{k+1}} \beta_k \beta_{k+1} dx, \qquad k = 1, \cdots, N-2.$$

The ordinary differential system (27) is exactly the same as the moving finite element scheme in [28]. The scheme was originally derived through a L^2 projection of a partial differential equation in the tangential space of u_h. There one needs to compute the inner product of a Dirac function and a discontinuous function, which is not well-defined even in a distribution sense. Our derivation is much simpler than that in [28]. In this sense, the Onsager principle gives a natural variational framework for the moving finite element method.

3.3 The stabilized scheme

The coefficient matrix in (27) may degenerate for some function $u_h \in V_h^N$. This is because the dissipation function Φ_h is a semi-positive definite quadratic form with respect to $\dot{u}_k$ and $\dot{x}_k$. The semi-positive definiteness is related to the degeneracy of the manifold V_h^N. For example, if we set $u_0(t) = u_1(t) = \cdots = u_N(t) = 0$, then $u_h(x,t) \equiv 0$ for all possible choice of X. That implies $\partial_t u_h \equiv 0$ and $\Phi_h \equiv 0$ for some nonzero $\dot{x}_k$.

To overcome the degeneracy of the system (27), we add a stabilized term as follows,

$$\Phi_h^\delta = \Phi_h + \frac{\delta\xi}{2} \sum_{k=1}^{N-1} \dot{x}_k^2, \tag{28}$$

where $\delta > 0$ is a small stabilization parameter. Other stabilizations can also apply, c.f. [27]. With the modified dissipation function Φ_h^δ, by the Onsager principle, $\dot{u}_k$ and $\dot{x}_k$ are obtained by

$$\min_{\dot{u}_k, \dot{x}_k} \Phi_h^\delta + \dot{\mathcal{E}}_h. \tag{29}$$

This leads to a modified system

$$\begin{cases} \frac{\partial \Phi_h^\delta}{\partial \dot{u}_k} + \frac{\partial \mathcal{E}_h}{\partial u_k} = 0, & k = 1, \cdots, N-1; \\ \frac{\partial \Phi_h^\delta}{\partial \dot{x}_k} + \frac{\partial \mathcal{E}_h}{\partial x_k} = 0, & k = 1, \cdots, N-1. \end{cases} \tag{30}$$

Once again it is an ordinary differential system for $\{u_k(t), x_k(t) \mid k = 1, \cdots N-1\}$. The explicit form of the system (30) is

$$\begin{pmatrix} \mathbf{A} & \mathbf{B} \\ \mathbf{B} & \mathbf{C} + \delta \mathbf{I} \end{pmatrix} \begin{pmatrix} \dot{\mathbf{u}} \\ \dot{\mathbf{x}} \end{pmatrix} = \begin{pmatrix} \mathbf{f} \\ \mathbf{g} \end{pmatrix}. \tag{31}$$

The positive definiteness of the coefficient matrix $\mathbf{M}_\delta := \begin{pmatrix} \mathbf{A} & \mathbf{B} \\ \mathbf{B} & \mathbf{C} + \delta \mathbf{I} \end{pmatrix}$ is given by the following lemma.

Lemma 3.2. *For any given $\delta > 0$, $X(t) = \{a = x_0 < x_1(t) < \cdots < x_{N-1}(t) < x_N = b\}$, and $\{u_k(t) | k = 1, \cdots, N-1\}$, the coefficient matrix $\mathbf{M}_\delta$ is positive definite.*

Proof. For any $\mathbf{y} \in R^{2(N-1)}$, we can denote it as $\mathbf{y} = \begin{pmatrix} \mathbf{y}_1 \\ \mathbf{y}_2 \end{pmatrix}$, where $\mathbf{y}_i \in R^{N-1}$, $i = 1, 2$. We suppose $\mathbf{y} \neq 0$. If $\mathbf{y}_2 \neq 0$, we can have

$$\mathbf{y}^T \mathbf{M}_\delta \mathbf{y} = \mathbf{y}^T \mathbf{M}_0 \mathbf{y} + \delta \mathbf{y}_2^T \mathbf{y}_2 \geq \delta \mathbf{y}_2^T \mathbf{y}_2 > 0. \tag{32}$$

where $\mathbf{M}_0 = \begin{pmatrix} \mathbf{A} & \mathbf{B} \\ \mathbf{B} & \mathbf{C} \end{pmatrix}$ and we have used the fact that

$$\mathbf{y}^T \mathbf{M}_0 \mathbf{y} = \Phi_h(u_1, \cdots, u_{N-1}, x_1, \cdots, x_{N-1}; \mathbf{y}_1, \mathbf{y}_2)$$

is semi-positive definite by its definition (24). Otherwise, if $\mathbf{y}_2 = 0$, then $\mathbf{y}_1 \neq 0$. We have

$$\mathbf{y}^T \mathbf{M}_\delta \mathbf{y} = \mathbf{y}_1^T \mathbf{A} \mathbf{y}_1 > 0, \tag{33}$$

for any given partition $\mathcal{T}(X(t))$ of the interval I, since the matrix $\mathbf{A}$ is the standard mass matrix of the linear finite element method with respect to the partition $\mathcal{T}(X(t))$ and thus positive definite. Combine the analysis together, we show that $\mathbf{M}_\delta$ is positive definite. □

By this lemma, the ODE system (31) can be rewritten as

$$\begin{pmatrix} \dot{\mathbf{u}} \\ \dot{\mathbf{x}} \end{pmatrix} = \mathbf{M}_\delta^{-1} \begin{pmatrix} \mathbf{f} \\ \mathbf{g} \end{pmatrix}. \tag{34}$$

The equation has a unique solution for any initial value $\mathbf{u}(0)$ and $\mathbf{x}(0)$ when the right hand side function $\begin{pmatrix} \mathbf{f}(\mathbf{u}, \mathbf{x}) \\ \mathbf{g}(\mathbf{u}, \mathbf{x}) \end{pmatrix}$ is Lipschitz continuous with respect to $\mathbf{u}$ and $\mathbf{x}$.

Remark 3.1. *The stiffness of the system and its numerical solution has been analyzed in [27, 36]. When the numerical solution is non-degenerate in V_h^N, the stabilization parameter δ can be chosen as zero. In general, δ can be chosen as a constant smaller than N^{-1}, where N is the maximal number of nodes in the discretization [28].*

Remark 3.2. *In real simulations, the mesh size in the MFEM can be very small if the numerical solution has sharp transition layers. In [27], a technique by adding "internodal spring force" was developed to avoid too small mesh size. We can use a similar technique by adding a penalty term to the total energy. We replace $\mathcal{E}(v_h)$ by*

$$\mathcal{E}_{\tilde{\delta}}(v_h) = \mathcal{E}(v_h) + \frac{\tilde{\delta}}{N} \sum_{k=0}^{N} (\ln(N h_k / L))^2. \tag{35}$$

where $h_k = x_{k+1} - x_k$, $L = b - a$ and $\tilde{\delta}$ is a small parameter. The penalty term goes to infinity when h_k goes to zero. In simulations, we can choose $\tilde{\delta}$ as a small parameter of order $O(\varepsilon^2)$, where ε is the thickness of the possible inner layer of the solution. If there is no inner layer in the solution, we can choose $\tilde{\delta}$ of order $O(\mathcal{E}_0/N)$ where $\mathcal{E}_0$ is the characteristic scale of the minimal energy $\mathcal{E}$. Since the penalty term is much smaller than the first term $\mathcal{E}(v_h)$, we will not consider it in the analysis next section for simplicity.

4 Numerical analysis

One important advantage of nonlinear approximations is that they have better accuracy than linear approximations. This is illustrated in Lemma 3.1 for the interpolation error. One would expect that the MFEM also has better accuracy than the standard FEM. However, the theoretical analysis is very difficult. In this section, we consider only the stationary solution when t goes to infinity.

4.1 The energy decay property

We first prove the following discrete energy decay property of the ordinary differential system (31).

Theorem 4.1. *Let* $(\mathbf{u}(t), \mathbf{x}(t))$ *be the solution of the equation* (31) *and* $u_h(t,x) \in V_h^N$ *be the corresponding piecewise linear function. Then we have*

$$\frac{d\mathcal{E}(u_h)}{dt} \leq 0, \tag{36}$$

where the equality holds only when $\dot{x}_k = 0$ *and* $\dot{u}_k = 0$ *for* $k = 1, \cdots, N-1$.

Proof. Notice that

$$\frac{d\mathcal{E}(u_h)}{dt} = \sum_{k=1}^{N-1}(\frac{\partial \mathcal{E}_h}{\partial u_k}\dot{u}_k + \frac{\partial \mathcal{E}_h}{\partial x_k}\dot{x}_k) = -\xi \sum_{k=1}^{N-1}(f_k\dot{u}_k + g_k\dot{x}_k) = -\xi(\dot{\mathbf{u}}^T, \dot{\mathbf{x}}^T)\mathbf{M}_\delta \begin{pmatrix} \dot{\mathbf{u}} \\ \dot{\mathbf{x}} \end{pmatrix},$$

where we have used the equation (31). By Lemma 3.2, we finish the proof of the theorem. □

From the proof, we easily see that

$$\frac{d\mathcal{E}(u_h)}{dt} = -2\Phi_h^\delta. \tag{37}$$

This implies the semi-discrete problem (31) preserves the energy dissipation structure (9) of the original gradient flow system.

4.2 Error analysis for the equilibrium state

We now consider the stationary solution of (15). When t goes to infinity, we suppose the solution $u(t,x)$ of (15) converge to a function $u^\infty(x)$ satisfying

$$\int_I \alpha \partial_x u^\infty \partial_x v + f(x, u^\infty) v \mathrm{d}x = 0, \qquad \forall v \in H_0^1(I). \tag{38}$$

To do analyse for this problem, we need one more assumption for the Lipschitz constant L_0 in (14) that

(H1) $$\alpha - L_0 c_0^2 > c_1, \qquad \text{for some constant } c_1 > 0,$$

where c_0 is a constant in the Poincare inequality

$$\|u\|_{L^2(I)} \leq c_0 |u|_{H^1(I)}. \tag{39}$$

Under this assumption, it is easy to see that the equation (38) is elliptic and has a unique solution. Furthermore, u^∞ is the unique minimizer for the energy minimization problem

$$\inf_{v \in H_0^1} \mathcal{E}(v). \tag{40}$$

In the following, we consider the approximation of the problem (38) by the MFEM. For the stationary solution for the discrete problem (31), we have the following theorem.

Theorem 4.2. *Let* $(\mathbf{u}(t), \mathbf{x}(t))$ *be the solution of the equation* (31) *which corresponds to a nondegenerate function* $u_h(t,x) \in V_h^N$. *When* t *goes to infinity,* $(\mathbf{u}(t), \mathbf{x}(t))$ *will converge to a vector* $(\mathbf{u}^\infty, \mathbf{x}^\infty)$. *Suppose that* $\mathbf{x}^\infty$ *corresponds to a partition of* I, *then* $u_h(t,x)$ *converges to a function* $u_h^\infty(x) \in V_h^N$ *which satisfies*

$$\begin{cases} \int_I \alpha \partial_x u_h^\infty \partial_x \phi_k + f(x, u_h^\infty)\phi_k dx = 0, & k = 1, \cdots, N-1, \\ \int_I \alpha \partial_x u_h^\infty \partial_x \beta_k + f(x, u_h^\infty)\beta_k dx - \frac{\alpha}{2}[(\partial_x u_h^\infty)^2]|_{x_k^\infty} = 0, & k = 1, \cdots, N-1. \end{cases} \tag{41}$$

Furthermore, if u_h^∞ *is nondegenerate and asymptotic stable, it is a local minimizer of* $\mathcal{E}(u_h)$ *in* V_h^N.

Proof. By Equation (37), we have the energy decay property

$$\frac{d\mathcal{E}(u_h(t))}{dt} = -2\Phi(\partial_t u_h) - \delta\xi \sum_{k=1}^N \dot{x}_k^2 \le 0, \qquad \forall t > 0.$$

Therefore, we have

$$\mathcal{E}(u_h(T)) = \mathcal{E}(u_h(0)) - \xi \int_0^T \int_I (\partial_t u_h)^2 dx dt - \delta\xi \sum_{k=1}^N \int_0^T \dot{x}_k^2 dt, \qquad \text{for } T > 0. \tag{42}$$

Notice that

$$\mathcal{E}(u_h(T)) \ge \inf_{v_h \in V_h^N} \mathcal{E}(v_h) \ge \inf_{v \in H_0^1(I)} \mathcal{E}(v) = \mathcal{E}(u^\infty).$$

Thus $\mathcal{E}(u_h(T))$ is bounded from below when T goes to infinity. By Equation (42), we have $\lim_{t\to\infty} \dot{x}_k(t) = 0$ and $\lim_{t\to\infty} \int_I (\partial_t u_h)^2 dx = 0$. Since x_k is in the bounded interval I, $x_k(t)$ converges when t goes to infinity. Similarly, $u_k(t)$ also converges when t goes to infinity. When the limit $\mathbf{x}^\infty$ generates a partition of I, then $(\mathbf{u}^\infty, \mathbf{x}^\infty)$ corresponds to a function u_h^∞ in V_h^N. From Equation (31), we have

$$\lim_{t\to\infty} f_k(\mathbf{u}, \mathbf{x}) = 0, \quad \lim_{t\to\infty} g_k(\mathbf{u}, \mathbf{x}) = 0, \qquad \text{for } k = 1, \cdots, N-1.$$

This leads to the equation (41), i.e. u_h^∞ is a critical point of the energy $\mathcal{E}(\cdot)$ in the manifold V_h^N.

When u_h^∞ is nondegenerate and asymptotic stable, it is a local minimizer of $\mathcal{E}$ in V_h^N. Otherwise, if it is a critical point but not a local minimizer of $\mathcal{E}$, there exists a non-trivial trajectory near u_h^∞ which makes the energy nondecreasing. This contradicts with the energy decay property in Theorem 4.1. □

Remark 4.1. *If* $\mathcal{E}(u)$ *has a quadratic form, Equation* (38) *is a linear equation. Then the theorem implies that* u_h^∞ *is a locally best approximation in energy norm. For example, suppose*

$$\mathcal{E}(u) = \int_I \frac{\alpha}{2}(\partial_x u)^2 + f(x)u \mathrm{d}x,$$

then by Equation (38), *we have*

$$\begin{aligned} \mathcal{E}(v_h) &= \int_I \frac{\alpha}{2}(\partial_x v_h)^2 + f(x)v_h \mathrm{d}x \\ &= \int_I \frac{\alpha}{2}(\partial_x v_h)^2 - \alpha \partial_x u^\infty \partial_x v_h \mathrm{d}x \\ &= \int_I \frac{\alpha}{2}(\partial_x v_h - \partial_x u^\infty)^2 dx - \int_I \frac{\alpha}{2}(\partial_x u^\infty)^2 \mathrm{d}x. \end{aligned}$$

Therefore, Theorem 4.2 implies that u_h^∞ is a locally best approximation of u^∞ in the energy norm when u_h^∞ is nondegenerate and asymptotic stable. This is one main result obtained in [20].

Notice the admissible set V_h^N for the discrete function is a $2(N-1)$ dimensional manifold in $H_0^1(I)$. In general the energy minimization problem $\mathcal{E}(\cdot)$ in the manifold V_h^N is not convex, even when $\mathcal{E}(\cdot)$ is a convex functional. This is very different from the standard FEM, noticing that the minimizer of a convex functional in a linear space is unique. Therefore, the local best approximations given in Theorem 4.2 is optimal. However, when the initial value is in the domain of attraction of a global minimizer of $\mathcal{E}(\cdot)$ in V_h^N, one can approximate the global minimizer by the MFEM. The following theorem shows that the global minimizer has an optimal convergence order.

Theorem 4.3. *Let u_h^∞ be a global minimizer of $\mathcal{E}(\cdot)$ in V_h^N. Assume that $f(x,u)$ is differentiable with respect to u. If $u^\infty \in B_q^{s+1}(L_q(I))$ with $0 \le s \le 1$ and $1/q < s + 1/2$, then we have*

$$|u^\infty - u_h^\infty|_{H^1} \lesssim N^{-s} |u^\infty|_{B_q^{s+1}(L_q(I))}. \tag{43}$$

Proof. Denote $w = u_h^\infty - u^\infty$. Since $u_h^\infty \in V_h^N \subset H_0^1(I)$ and u^∞ is the minimizer of $E(u)$ in $H_0^1(I)$, then we have $w \in H_0^1(I)$ and

$$\begin{aligned}
&\mathcal{E}(u_h^\infty) - \mathcal{E}(u^\infty) \\
&= \int_I \Big(\frac{\alpha}{2}(\partial_x u_h^\infty)^2 - \frac{\alpha}{2}(\partial_x u^\infty)^2 \Big) + \Big(F(x, u_h^\infty) - F(x, u^\infty) \Big) \mathrm{d}x \\
&= \int_I \frac{\alpha}{2}(\partial_x w)^2 + \alpha \partial_x u^\infty \partial_x w + f(x, u^\infty) w + \frac{1}{2} \partial_u f(x, u^\infty + sw) w^2 \mathrm{d}x \\
&= \int_I [\alpha \partial_x u^\infty \partial_x w + f(x, u^\infty) w] + \frac{\alpha}{2}(\partial_x w)^2 + \frac{1}{2} \partial_u f(x, u^\infty + sw) w^2 \mathrm{d}x \\
&= \int_I \frac{\alpha}{2}(\partial_x w)^2 + \frac{1}{2} \partial_u f(x, u^\infty + sw) w^2 \mathrm{d}x,
\end{aligned} \tag{44}$$

where $0 \le s \le 1$ and we have used the equation (38) in the last equation. From the Lipschitz condition (14) of f, we know that $|\partial_u f(x,u)| \le L_0$. This further leads to

$$\begin{aligned}
\mathcal{E}(u_h^\infty) - \mathcal{E}(u^\infty) &\ge \int_I \frac{\alpha}{2}(\partial_x w)^2 \mathrm{d}x - \frac{L_0}{2} \int_I w^2 \mathrm{d}x \\
&\ge \frac{\alpha - L_0 c_0^2}{2} \int_I (\partial_x w)^2 \mathrm{d}x \\
&\ge \frac{c_1}{2} \int_I (\partial_x w)^2 \mathrm{d}x = \frac{c_1}{2} |\partial_x u^\infty - \partial_x u_h^\infty|_{H^1}^2.
\end{aligned} \tag{45}$$

Here we have used assumption (H1) and the Poincare inequality (39).

For any $v_h \in V_h^N$, we denote $\tilde{w} = v_h - u^\infty$. Noticing that u_h^∞ is a global minimizer of $\mathcal{E}$, similar calculations as (44) gives

$$\begin{aligned}
\mathcal{E}(u_h^\infty) - \mathcal{E}(u^\infty) &\le \mathcal{E}(v_h) - \mathcal{E}(u^\infty) \\
&= \int_I \frac{\alpha}{2}(\partial_x \tilde{w})^2 + \frac{1}{2} \partial_u f(x, u^\infty + s\tilde{w}) \tilde{w}^2 \mathrm{d}x \\
&\lesssim \|u^\infty - v_h\|_{H^1}^2, \qquad \forall v_h \in V_h^N.
\end{aligned}$$

Combine the inequality with (45) and using the Poincare inequality again, we obtain

$$|u^\infty - u_h^\infty|_{H^1}^2 \lesssim \mathcal{E}(u_h^\infty) - \mathcal{E}(u^\infty) \lesssim \inf_{v_h \in V_h^N} \|u^\infty - v_h\|_{H^1}^2 \lesssim (\sigma_N(u))^2. \tag{46}$$

By Lemma 3.1, we have finished the proof.

□

In general it is not clear how to determine the domain of attraction of a global minimizer. There is no guarantee that all initial values can tend to a globally stationary solution. As suggested by the numerical results in [20], it is possible that the solution of a MFEM does not go to the global minimizer when some elements in the partition tend to degenerate.

5 Numerical Examples

In the following, we show some numerical examples. In our simulations, we solve the problem (31) with a modified energy (35) by a simple forward Euler scheme with very small time step. More efficient solvers(e.g. some implicit stiff ODE solver) have been studied in [27].

5.1 A linear diffusion equation

We first consider a linear diffusion problem:

$$\begin{cases} \partial_t u - \partial_{xx} u = f(x), & x \in (a,b), t > 0; \\ u(x,0) = u_0(x), & x \in (a,b); \\ u(a,t) = u(b,t) = 0 & t > 0. \end{cases} \tag{47}$$

This corresponding energy density is given by

$$\mathcal{E}(u) = \int_I \frac{1}{2}|\partial_x u|^2 - f(x)u(x)\mathrm{d}x, \tag{48}$$

where $I = (a,b)$. We choose $\delta = 0.0001$ and $\tilde{\delta} = 0.01$. We test for several different u_0 and f.

Example 1. In the first example, we set $I = (0,1)$ and $f(x) = \delta_{a_0}(x)$ which is a Dirac measure at the middle point $a_0 = 0.5$. We have $\int_0^1 f(x)v(x)\mathrm{d}x = v(x_0)$, for any $v \in C_0^1([0,1])$. The initial solution is given by $u_0 = \sin(\pi x) + x\chi_{\{x<x_0\}} + (1-x)\chi_{\{x>x_0\}}$. In this case the equation (47) has an analytic solution

$$u(x,t) = \sin(\pi x)e^{-\pi^2 t} + x\chi_{\{x<x_0\}} + (1-x)\chi_{\{x>x_0\}}.$$

The spacial derivative of the solution has a jump at the middle point $a_0 = 0.5$.

The initial partition of I is uniform and given by $0 = x_0 < \frac{1}{N} < \cdots < \frac{N-1}{N} < x_N = 1$. Here we choose $N = 5, 9, 19, 39, 79$ so that the non-smooth point a_0 is not a node in the initial partition. We solve the problem (31) until $T = 0.04$. The H^1 error and the L^2 error between the discrete solution u_h and the exact solution u at T are computed by

$$err_{H^1} := \Big(\int_I (\partial_x u(x,T) - \partial_x u_h(x,T))^2 \mathrm{d}x \Big)^{1/2},$$
$$err_{L^2} := \Big(\int_I (u(x,T) - u_h(x,T))^2 \mathrm{d}x \Big)^{1/2}.$$

Table 1: The H^1-norm and L^2-norm of the error in Experiment 1.

Adaptive	err_{H^1}	order	err_{L^2}	order
$N = 5$	0.3326	–	0.0338	–
$N = 9$	0.1571	1.28	0.0098	2.11
$N = 19$	0.0842	0.83	0.0022	2.00
$N = 39$	0.0470	0.81	0.000523	1.99
$N = 79$	0.0265	0.81	0.000141	1.86

Uniform	err_{H^1}	order	err_{L^2}	order
$N = 5$	0.6363	–	0.0435	–
$N = 9$	0.1571	0.72	0.0153	1.77
$N = 19$	0.2587	0.64	0.0043	1.70
$N = 39$	0.1703	0.58	0.0013	1.66
$N = 79$	0.1159	0.54	0.000438	1.54

In Table 1, we show the numerical errors for the different choice of N. The convergence order is computed by $s_i := \ln(err_i/err_{i+1})/\ln(N_{i+1}/N_i)$, which implies that the errors decrease with order $O(N^{-s})$. We can see that the H^1-error is almost of order $O(N^{-0.8})$, close to the optimal convergence rate $O(N^{-1})$. Meanwhile, the L^2-error is of order $O(N^{-2})$, which is optimal in approximation theory. In comparison, we also show the errors computed by the standard finite element method on a uniform partitions of I. We could see that the H^1 norm is almost of order $O(N^{-0.5})$ and the L^2-error is of order $O(N^{-1.5})$. This is reasonable since the exact solution is not smooth. In this case, the MFEM has better accuracy than the standard FEM.

In Figure 1 we illustrate the numerical solutions for the case $N = 9$ at different time t. We can see that initially the interval I is uniformly divided into $N - 1$ cells and u_k are simply the interpolation of $u(0, x)$. There is a large error at $a_0 = 0.5$ since the initial function is not smooth there. With time increasing, we can see that the notes x_k move with time. In particular, the two notes near the non-smooth point a_0 approach to the point gradually. The distance between them become smaller and smaller. At about $t = 0.0048$, the right point almost arrives at a_0. After that, the left point moves away from the point to further decrease the computational error.

Example 2. To further illustrate the behaviour of the MFEM, we consider a diffusion problem with an almost singular initial condition. We set $f = 0$ and $I = (-3, 3)$. We choose $u_0 = \frac{1}{\sqrt{0.004\pi}}(e^{-x^2/(0.004)} - e^{-9/(0.004)})$, which is a very sharp Gaussian function as shown in the first sub-figure in Figure 2. u_0 is almost equal to zero outside of a narrow interval. For this problem, we do not have an explicit formula for the analytic solution.

Initially we choose a grid whose points concentrated in a small interval $(-0.2, 0.2)$ to resolve the profile of u_0:

$$X(0) = \{-3, -0.2, \cdots, -0.2 + i\frac{0.4}{N-2}, \cdots, 0.2, 3\}.$$

In Figure 2, we show the numerical solution when $N = 19$. We can see that the numerical solutions spread outwards gradually while the height of the profile decreases. In particular, the grid points gradually adjust their positions so that the Gaussian profile of the numerical solution is always well resolved.

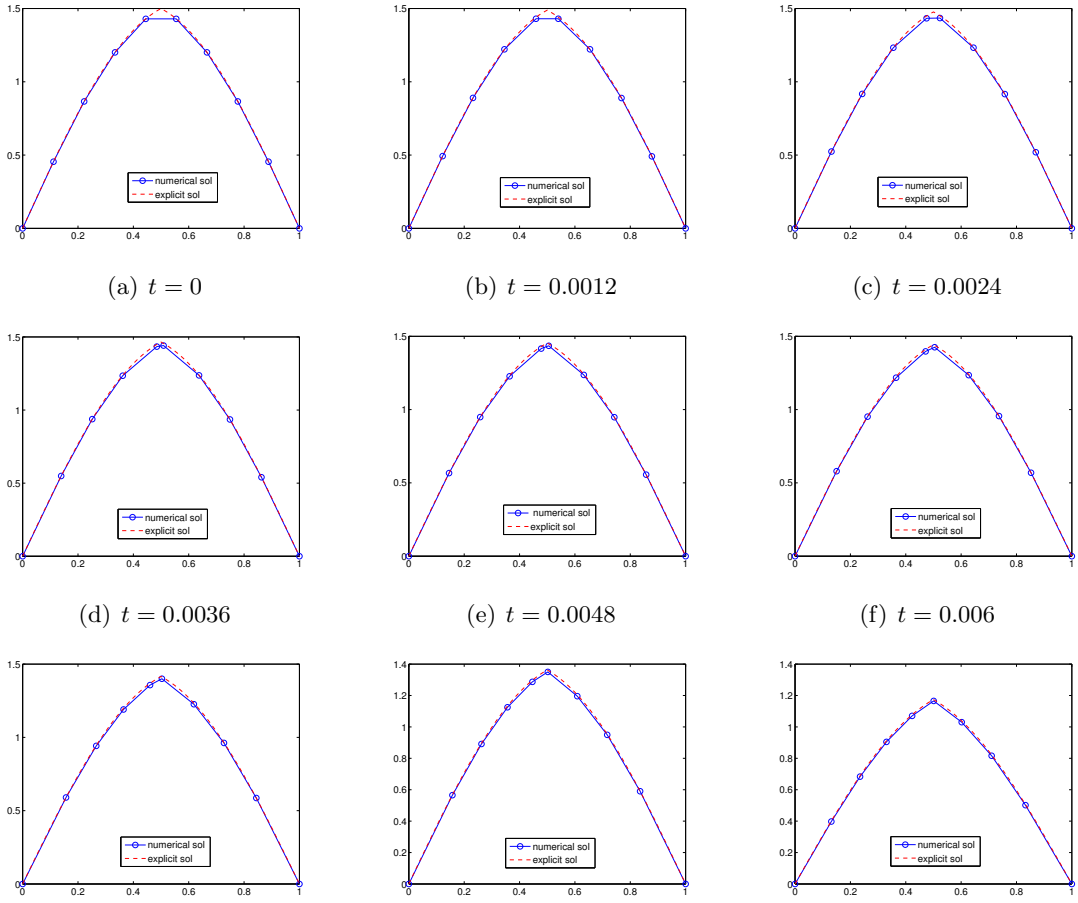

(a) $t = 0$ (b) $t = 0.0012$ (c) $t = 0.0024$

(d) $t = 0.0036$ (e) $t = 0.0048$ (f) $t = 0.006$

(g) $t = 0.009$ (h) $t = 0.014$ (i) $t = 0.04$

Figure 1: The profile of the numerical solution and the exact solution at different time t when $N = 9$ for Example 1. The small circles in the figures show the computational solutions u_k corresponding to x_k, for $k = 0, \cdots, 9$.

5.2 The Allen-Cahn equation

We then consider an Allen-Cahn equation in a interval $I = (0, 1)$,

$$\begin{cases} \partial_t \phi - \varepsilon \partial_{xx} \phi + \frac{\phi^3 - \phi}{\varepsilon} = 0, & x \in (0,1), \\ \phi(x, 0) = x, & x \in (0,1), \\ \phi(0, t) = 0, \phi(1, t) = 1, \end{cases} \tag{49}$$

which is a nonlinear example for the model problem (15). The corresponding free energy is

$$\mathcal{E}(\phi) = \int_0^1 \frac{\varepsilon}{2} (\partial_x \phi)^2 + \frac{(1 - \phi^2)^2}{4\varepsilon} \mathrm{d}x. \tag{50}$$

We are interested in the stationary profile of the problem. When ε is small enough, the profile is approximated nicely by

$$\phi^\infty(x) = \tanh(\frac{x - 0.5}{\sqrt{2}\varepsilon}). \tag{51}$$

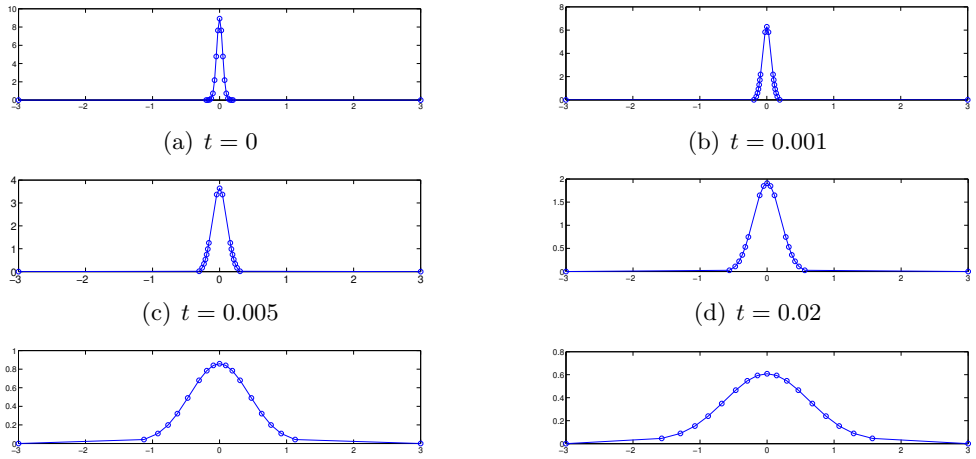

(a) $t = 0$ (b) $t = 0.001$

(c) $t = 0.005$ (d) $t = 0.02$

(e) $t = 0.1$ (f) $t = 0.2$

Figure 2: The profile of the numerical solution at different time t when $N = 19$ for Example 2. The small circles in the figures show the computational solutions u_k corresponding to x_k, for $k = 0, \cdots, 19$.

It has a very thin inner layer at the middle point $x = 0.5$. In simulations, we choose $\delta = 0.0001$, $\tilde{\delta} = 0.0001$ and test for different values of ε. The initial condition is given by

$$\phi(0, x) = 2(x - 0.5).$$

Example 3. In this example, we set $\varepsilon = 0.05$ and test the method for different choice of N. Initially, we give a uniform partition of I that $X(0) = \{0 = x_0 < \frac{1}{N} < \cdots < \frac{N-1}{N} < x_N = 1\}$, We solve the problem for various choices of $N = 5, 10, 20, 40, 80$.

In the computation, the profile of ϕ_h changes gradually to a stationary state ϕ_h^∞. Meanwhile the grid points move into a highly non-uniform distribution to resolve the inner layers of the solution. We illustrate some plots of the final solution ϕ_h^∞ as well as the distributions of x_k in Figure 3. They are obtained by solving the problem (31) until the decrease of the discrete energy in one step is smaller than a tolerance $TOL = 1e^{-10}$. The profile of the "exact" solution ϕ^∞ is also shown. We can see that the numerical solution fits the exact solution very well even on a very coarse mesh($N = 5$). Almost all the grid points are distributed in the inner layer of the solution. Interestingly, it seems that the nodes are dense where the second order derivative of the solution is large. This indicates a uniform distribution of the errors in H^1 norm.

In Table 2, we illustrate the H^1 error between ϕ_h^∞ and ϕ^∞:

$$err_{H^1} := \Big(\int_I (\partial_x \phi^\infty(x) - \partial_x \phi_h^\infty(x))^2 \mathrm{d}x \Big)^{1/2}.$$

It seems that the H^1 errors decrease with order $O(N^{-1})$. This is optimal for free-knot piecewise linear functions. This is consistent with the analytical results in the Section 4. In addition, we also compute the errors of the minimal energies by computing

$$err_{eng} = |\mathcal{E}(\phi_h^\infty) - \sigma|,$$

where $\sigma = \frac{2\sqrt{2}}{3}$ is the total energy corresponding to the profile ϕ^∞. We see that the errors of the energy decrease with order $O(N^{-2})$.

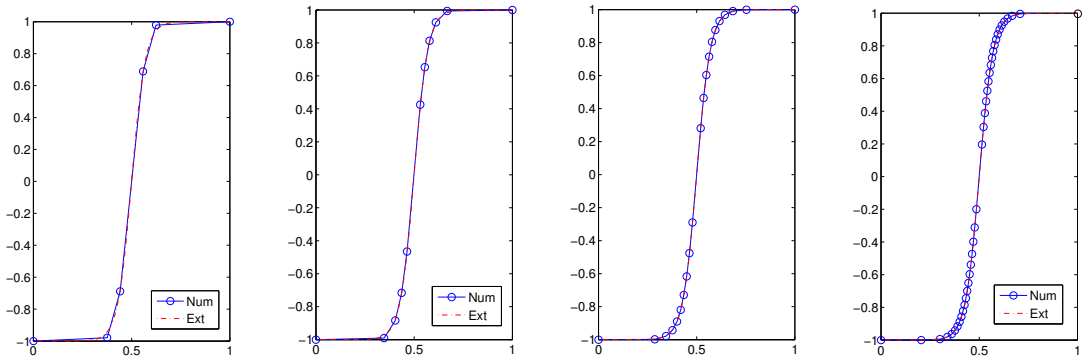

(a) $N = 5$ (b) $N = 10$ (c) $N = 20$ (d) $N = 40$

Figure 3: The numerical solutions of the Allen-Chan equation in stationary sate with $\varepsilon = 0.05$ for various $N = 5, 10, 20, 40$. The small circles in the figures mark the points $(x_k, \phi_{h,k})$.

Table 2: The H^1 errors of the stationary profile and the errors of the minimial energies in Example 3.

Adaptive	err_{H^1}	order	err_{eng}	order
$N = 5$	1.0004	–	0.0264	–
$N = 10$	0.5025	0.99	0.00646	2.03
$N = 20$	0.2641	0.93	0.00175	1.88
$N = 40$	0.1268	1.06	0.000402	2.12
$N = 80$	0.0691	0.88	0.000120	1.87

Example 4. In the last example, we test for a smaller $\varepsilon = 0.01$, which corresponds to a sharper inner layer. All other setups are the same as in the previous example.

In Figure 4, we show the the stationary solutions of the Allen-Cahn equation for various different choice of N. We see that the very sharp inner layer is resolved nicely by the moving finite element method even when $N = 5$. In Table 3, we show the H^1 errors between ϕ_h^∞ and $\phi^\infty(x)$ and also the errors of the minimal energy. We see that the H^1 errors decrease with order $O(N^{-1})$ and the errors of the energies are of order $O(N^{-2})$. Both of them are optimal. This again verifies the theoretical results in the previous section.

Table 3: The H^1 errors of the stationary profile and the errors of the minimial energies in Example 4.

Adaptive	err_{H^1}	order	err_{eng}	order
$N = 5$	2.2779	–	0.0281	–
$N = 10$	1.7365	0.39	0.0067	2.07
$N = 20$	0.8043	1.11	0.0017	1.98
$N = 40$	0.3728	1.11	0.000467	1.86
$N = 80$	0.1641	1.18	0.000135	1.79

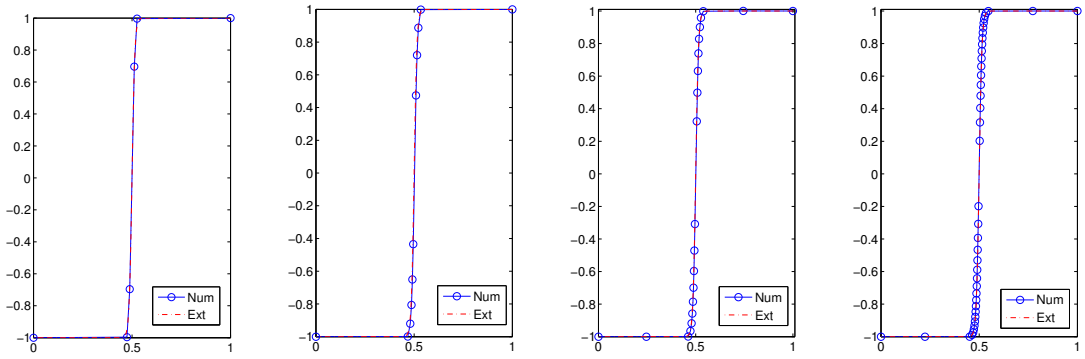

(a) $N = 5$ (b) $N = 10$ (c) $N = 20$ (d) $N = 40$

Figure 4: The numerical solutions of the Allen-Chan equation in stationary sate with $\varepsilon = 0.01$ for various $N = 5, 10, 20, 40$. The small circles in the figures mark the points $(x_k, \phi_{h,k})$.

6 Conclusions

We show that the Onsager principle can act as a variational framework for the MFEM for a gradient flow system. The derivation of the method using the principle is much easier than the original approach in [28]. The discrete problem has the same energy dissipation structure as the continuous one. This helps us to do numerical analysis for a long time(stationary) solution of the gradient flow system. Under some conditions, we prove that the MFEM gives locally best approximation for the energy. The optimal convergence rate can be obtained if a global minimizer is detected in the free-knot piecewise linear function space. Although we consider only the one dimensional case, the analysis can be generated to high dimensional problems directly. In addition, it is also possible to consider more complicated gradient flows.

In this paper, we restrict our analysis on the stationary solution, although numerical experiments show that the method has optimal convergence rate for time dependent solutions (at least) for the linear diffusion problem. Numerical analysis for the dynamic problems will be left for future study.

Acknowledgment

This work was supported in part by NSFC grants DMS-11971469 and the National Key R&D Program of China under Grant 2018YFB0704304 and Grant 2018YFB0704300.

References

[1] M. J. Baines. *Moving Finite Elements*. Clarendon Press, Oxford, 1994.

[2] M. J. Baines, M. Hubbard, and P. Jimack. A moving mesh finite element algorithm for the adaptive solution of time-dependent partial differential equations with moving boundaries. *Applied Numerical Mathematics*, 54(3-4):450–469, 2005.

[3] R. E. Bank and M. S. Metti. A diagonally-implicit time integration scheme for space-time moving finite elements. *Journal of Computational Mathematics*, 37(3), 2019.

[4] P. Binev, W. Dahmen, and R. DeVore. Adaptive finite element methods with convergence rates. *Numerische Mathematik*, 97(2):219–268, 2004.

[5] P. Binev, W. Dahmen, R. DeVore, and P. Petrushev. Approximation classes for adaptive methods. *Serdica Mathematical Journal*, 28(4):391p–416p, 2002.

[6] C. J. Budd, W. Huang, and R. D. Russell. Adaptivity with moving grids. *Acta Numerica*, 18:111–241, 2009.

[7] W. Cao, W. Huang, and R. D. Russell. A moving mesh method based on the geometric conservation law. *SIAM Journal on Scientific Computing*, 24(1):118–142, 2002.

[8] N. N. Carlson and K. Miller. Design and application of a gradient-weighted moving finite element code I: in one dimension. *SIAM Journal on Scientific Computing*, 19(3):728–765, 1998.

[9] Q. Cheng, C. Liu, and J. Shen. A new interface capturing method for allen-cahn type equations based on a flow dynamic approach in lagrangian coordinates, i. one-dimensional case. *Journal of Computational Physics*, 419:109509, 2020.

[10] R. A. DeVore. Nonlinear approximation. *Acta numerica*, 7:51–150, 1998.

[11] R. A. DeVore and R. C. Sharpley. Besov spaces on domains in R^d. *Transactions of the American Mathematical Society*, 335(2):843–864, 1993.

[12] Y. Di, X. Xu, and M. Doi. Theoretical analysis for meniscus rise of a liquid contained between a flexible film and a solid wall. *Europhys. Lett.*, 113(3):36001, feb 2016.

[13] M. Doi. Onsager's variational principle in soft matter. *J. Phys.: Condens. Matter*, 23:284118, 2011.

[14] M. Doi. *Soft Matter Physics*. Oxford University Press, Oxford, 2013.

[15] M. Doi. Onsager principle as a tool for approximation. *Chin. Phys. B*, 24:020505, 2015.

[16] T. Dupont. Mesh modification for evolution equations. *Mathematics of Computation*, 39(159):85–107, 1982.

[17] W. Huang, Y. Ren, and R. D. Russell. Moving mesh partial differential equations (MMPDES) based on the equidistribution principle. *SIAM Journal on Numerical Analysis*, 31(3):709–730, 1994.

[18] W. Jiang, Q. Zhao, T. Qian, D. J. Srolovitz, and W. Bao. Application of Onsager's variational principle to the dynamics of a solid toroidal island on a substrate. *Acta Mater.*, 163:154–160, 2019.

[19] P. K. Jimack. On steady and large time solutions of the semi-discrete moving finite element equations for one-dimensional diffusion problems. *IMA journal of numerical analysis*, 12(4):545–564, 1992.

[20] P. K. Jimack. A best approximation property of the moving finite element method. *SIAM journal on numerical analysis*, 33(6):2286–2302, 1996.

[21] P. K. Jimack. Optimal eigenvalue and asymtotic large-time approximations using the moving finite-element method. *IMA journal of numerical analysis*, 16(3):381–398, 1996.

[22] R. Li, T. Tang, and P. Zhang. Moving mesh methods in multiple dimensions based on harmonic maps. *Journal of Computational Physics*, 170(2):562–588, 2001.

[23] C. Liu and Y. Wang. On lagrangian schemes for porous medium type generalized diffusion equations: A discrete energetic variational approach. *Journal of Computational Physics*, 417:109566, 2020.

[24] C. Liu and Y. Wang. A variational lagrangian scheme for a phase-field model: A discrete energetic variational approach. *SIAM Journal on Scientific Computing*, 42(6):B1541–B1569, 2020.

[25] S. Lu and X. Xu. An efficient diffusion generated motion method for wetting dynamics. *arXiv:2005.04710*, 2020.

[26] X. Man and M. Doi. Vapor-induced motion of liquid droplets on an inert substrate. *Phys. Rev. Lett.*, 119(4):044502, 2017.

[27] K. Miller. Moving finite elements. II. *SIAM Journal on Numerical Analysis*, 18(6):1033–1057, 1981.

[28] K. Miller and R. N. Miller. Moving finite elements. I. *SIAM Journal on Numerical Analysis*, 18(6):1019–1032, 1981.

[29] L. Onsager. Reciprocal relations in irreversible processes. I. *Phys. Rev.*, 37(4):405–426, feb 1931.

[30] L. Onsager. Reciprocal relations in irreversible processes. II. *Phys. Rev.*, 38(12):2265–2279, dec 1931.

[31] C.-V. Pao. *Nonlinear parabolic and elliptic equations*. Springer Science & Business Media, 2012.

[32] P. P. Petrushev. Direct and converse theorems for spline and rational approximation and besov spaces. In *Function spaces and applications*, pages 363–377. Springer, 1988.

[33] T. Qian, X.-P. Wang, and P. Sheng. A variational approach to moving contact line hydrodynamics. *J. Fluid Mech.*, 564:333–360, 2006.

[34] T. Tang. Moving mesh methods for computational fluid dynamics. *Contemporary mathematics*, 383(8):141–173, 2005.

[35] H. Triebel. *Interpolation theory, function spaces, differential operators*. North-Holland, 1978.

[36] A. J. Wathen and M. Baines. On the structure of the moving finite-element equations. *IMA Journal of Numerical Analysis*, 5(2):161–182, 1985.

[37] X. Xu, Y. Di, and M. Doi. Variational method for contact line problems in sliding liquids. *Phys. Fluids*, 28:087101, 2016.

[38] J. Zhou and M. Doi. Dynamics of viscoelastic filaments based on Onsager principle. *Phys. Rev. Fluids*, 3:084004, 2018.